

## Numerical analysis of a hybrid substructure for offshore wind turbines

Min-Su Park<sup>\*</sup>, Youn-Ju Jeong<sup>a</sup>, Young-Jun You<sup>b</sup>, Du-Ho Lee<sup>c</sup> and  
Byeong-Cheol Kim<sup>d</sup>

*Structural Engineering Research Division, Korea Institute of Civil Engineering and Building Technology,  
283Goyangdae-ro, Ilsanseo-gu, Goyang-si411-712, Republic of Korea*

*(Received July 3, 2014, Revised August 10, 2014, Accepted August 14, 2014)*

**Abstract.** For the reliable design of substructure supporting offshore wind turbines it is very important to reduce the effects of wave forces. Since the substructure is strongly influenced by the effects of wave forces as the size of substructure increases. In the present study, the hybrid substructure with multi-cylinder is newly suggested to reduce the effects of wave forces. Using diffraction theory the scattering waves in a fluid region are expressed by an Eigenfunction expansion method with three dimensional potential theory to calculate the wave force acting on the hybrid substructure. The wave force and wave run-up acting on the hybrid substructure is presented to examine the water wave interaction according to the variation of cylindrical size and the distance among cylinders. It is found that the suggested hybrid substructure with multi-cylinder is very useful to reduce the effects of wave forces acting on the substructure for offshore wind turbines.

**Keywords:** hybrid substructure; offshore wind turbine; Eigenfunction expansion method; wave force; wave run-up

---

### 1. Introduction

To tackle climate change and to find alternative and reliable energy sources, the offshore wind energy has gained attention from many countries. It is recognized that the offshore wind energy one of the most promising and fastest growing alternative energy sources in the world. Therefore, many offshore wind farms are in the planning phase. South Korea will also invest \$9 billion in building a 2.5GW offshore wind farm in the southwest sea of Korea by 2019 (South Korea offshore wind project plan 2011). However, the size of a substructure supporting offshore wind turbines is gradually increased because the size of a tower and a rotor-nacelle becomes larger with increment of wind turbine's gross generation. In other words, the substructure for offshore wind turbines is strongly influenced by the effect of wave forces as the size of substructure increases.

---

\*Corresponding author, Ph.D., E-mail: [mspark@kict.re.kr](mailto:mspark@kict.re.kr)

<sup>a</sup> Ph.D., E-mail: [yjjeong@kict.re.kr](mailto:yjjeong@kict.re.kr)

<sup>b</sup> Master, E-mail: [yjyou@kict.re.kr](mailto:yjyou@kict.re.kr)

<sup>c</sup> Master, E-mail: [ldh0067083@kict.re.kr](mailto:ldh0067083@kict.re.kr)

<sup>d</sup> Ph.D., E-mail: [bckim@kict.re.kr](mailto:bckim@kict.re.kr)

Therefore, it is very important to reduce the wave forces acting on substructures. In the present study the hybrid substructure, which is composed of multi-cylinder having different radius of each upper and lower area as shown in Fig. 1, is newly suggested to reduce the wave forces using water wave interaction with multi-cylinder.

The water wave interaction with multi-cylinder has been studied by many researchers. Under the assumption of potential flow and linear wave theory, Spring and Monkmeyer (1974) first proposed a semi-analytical solution for impermeable cylinders using an Eigenfunction expansion approach. In the case of  $N$  bottom-mounted circular cylinders Linton and Evans (1990) simplified this solution. Kagemoto and Yue (1986) developed another exact solution within the context of linearized theory, showing that a general three-dimensional wave diffraction problem could be solved in terms of algebraically-based diffraction characteristics of a single member. Another popular approach based on the wide-spacing assumption was the modified plane wave method, developed by McIver and Evans (1984). This approach was later applied to a variety of cases by McIver (1984), Williams and Demirebilek (1988), Williams and Abul-Azm (1989), and Williams and Rangappa (1994). Using Eigen-function expansion method, the interaction of waves with  $N$  vertical circular cylinders is examined by Kim (1993). For the analysis of  $N$  full-body porous-surfaced cylinders, the Eigen-function expansion method could be employed to describe hydrodynamic interactions in multi-body structures (Williams and Li 1998, 2000, Cho and Kim 2010, Park *et al.* 2010, Zhao *et al.* 2011). Cho *et al.* (2012) also presented the hydrodynamic performance of the wave energy converter (WEC) in various design parameters and irregular-wave conditions using Eigen-function expansion method.

In order to calculate the wave forces acting on the suggested hybrid substructure with multi-cylinder, the fluid domain is divided into two regions: an interior region and an exterior region. Using three-dimensional linear potential theory the scattering waves in each fluid region are expressed by the Eigenfunction expansion method. The comparison of wave forces and wave run-ups is made for the different depth ratio of interior region. In order to examine the water wave interaction with hybrid substructures, the wave forces and the wave run-ups are presented for the different array of hybrid substructures with multi-cylinder.

## 2. Formulation

A hybrid substructure for offshore wind turbines is composed of multi-cylinder having different radiuses of each upper and lower area as shown in Fig. 1. The hybrid substructure is situated in water of uniform depth  $d$  and the draughts of each upper and lower area are  $h$  and  $c$ , respectively. The lower and the upper radius of the  $j$ th cylinder are  $a_j$  and  $b_j$ , respectively. Also, the global Cartesian coordinate system  $(x, y, z)$  is defined with an origin located on the sea bed with the  $z$ -axis directed vertically upwards. The center of each cylinder at  $(x_j, y_j)$  is taken as the origin of a local polar coordinate system  $(r_j, \theta_j)$ , where  $\theta_j$  is measured counter-clockwise from the positive  $x$ -axis. The center of the  $l$ th cylinder has a polar coordinate  $(R_{jl}, \alpha_{jl})$  relative to the  $j$ th cylinder. The coordinate relationship between the  $j$ th and  $l$ th cylinder is shown in Fig. 1. Moreover, the fluid domain is divided into two regions: region 1 which is interior to the cylinder ( $b_j \leq r_j \leq a_j, d-h \leq z \leq d$ ) and region 2 which is exterior to the cylinder and extends to infinity in the horizontal plane ( $r_j \geq a_j, 0 \leq z \leq d$ ).

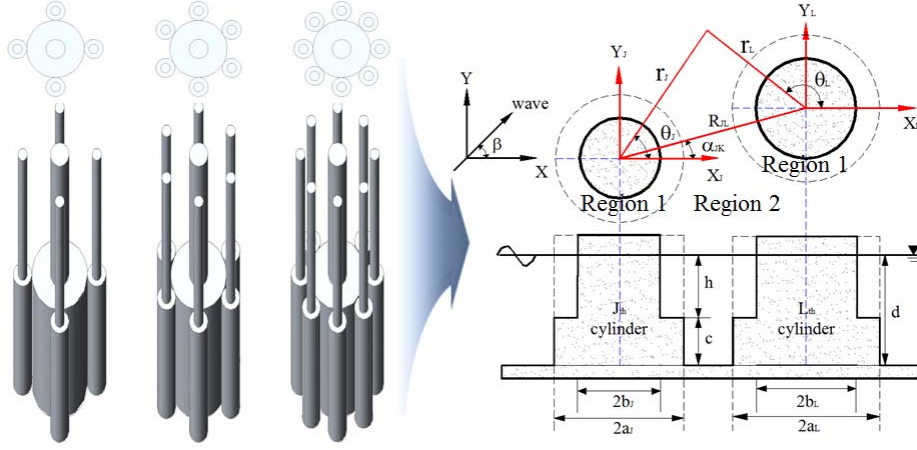


Fig. 1 Coordinate system for an array of hybrid substructures

It is assumed that the computational fluid domain is inviscid, and incompressible, and its motion is irrotational. The array of cylinders is subjected to a train of regular waves of height  $H$  and angular frequency  $\omega$  propagating at an angle  $\beta$  to the positive  $x$ -axis. The velocity potential of the computational domain can be written as

$$\Phi(x, y, z, t) = \text{Re} \left[ -\{igH / (2\omega)\} \phi(x, y, z) e^{-i\omega t} \right] \quad (1)$$

Where  $\text{Re}[\ ]$  denotes the real part of a complex velocity potential  $\Phi$ , and  $g$  is the gravitational acceleration.

As a governing equation, the Laplace equation is satisfied for the entire fluid domain of the present boundary value problem

$$\nabla^2 \phi = 0 \quad (2)$$

For solving the governing equation, the following boundary conditions for the free surface (Eq. (3)), bottom of region 1 (Eq. (4)), vertical wall of upper and lower area (Eq. (5)), flat rigid sea bottom (Eq. (6)), and the Sommerfeld radiation boundaries (Eq. (7)) can be given, respectively

$$\frac{\partial \phi}{\partial z} - \frac{\omega^2}{g} \phi = 0 \quad \text{on } z = d \quad (3)$$

$$\frac{\partial \phi}{\partial z} = 0 \quad \text{on } z = d - h, \quad b_j \leq r \leq a_j \quad (4)$$

$$\frac{\partial \phi}{\partial r_j} = 0 \quad \text{on } r = b_j, \quad (d - h) \leq z \leq d \quad (5)$$

$$\frac{\partial \phi}{\partial r_j} = 0 \quad \text{on } r = a_j, \quad 0 \leq z \leq (d - h)$$

$$\frac{\partial \phi}{\partial z} = 0 \quad \text{on } z = 0 \quad (6)$$

$$\lim_{r \rightarrow \infty} \sqrt{r} \left[ \frac{\partial}{\partial r} (\phi_2 - \phi_{in}) - ik (\phi_2 - \phi_{in}) \right] = 0 \quad (7)$$

where  $k$  is the incident wave number related to the wave frequency through the dispersion relation  $\omega^2 = gk \tanh kd$ , and  $d$  is the water depth.  $\phi_2$  and  $\phi_{in}$  denote the total velocity potential in region 2 and the incident wave potential, respectively.

The wave potential in the interior region (1) of the  $j$ th cylinder, which satisfies the appropriate free surface and structural boundary conditions, can be expressed by the following Eigen-function expansion

$$\phi_1^j = \sum_{n=-\infty}^{\infty} \left[ A_n^j J_n(k_0 r_j) - \frac{J_n'(k_0 b_j)}{Y_n'(k_0 b_j)} A_n^j Y_n(k_0 r_j) \right] \times \frac{\cosh \{k_0 (z - d + h)\}}{\cosh(k_0 h)} e^{in\theta} \quad (8)$$

in which  $J_n$  and  $Y_n$  denotes the Bessel function of the first and the second kind of order  $n$ , and  $J_n'$  and  $Y_n'$  are the first derivatives of the Bessel function, respectively.  $A_n^j$  is the unknown complex potential coefficient. A new wave number  $k_0$  is introduced, which satisfies the dispersion relation  $\omega^2 = gk_0 \tanh k_0 h$ , where  $h$  denote local water depth in the interior region 1.

The incident wave potential in the  $j$ th local polar coordinate system can be expressed using Jacobi-Anger expansion of Bessel function as follows

$$\phi_{in}^j = \frac{\cosh kz}{\cosh kd} T_j \sum_{n \rightarrow -\infty}^{\infty} J_n(kr_j) e^{in(\pi/2 + \theta_j - \beta)} \quad (9)$$

where  $T_j = e^{ik(x_j \cos \beta + y_j \sin \beta)}$  is a phase factor associated with the cylinder  $j$  from the global origin.

The wave potential in the exterior region (2), which is expressed by using Graf's addition theorem for the Bessel Functions (Abramowitz and Stegun 1972) and satisfies the Helmholtz equation, can be expressed by the following Eigenfunction expansion

$$\phi_2^j(r_j, \theta_j) = \sum_{n=-\infty}^{\infty} \left[ e^{ik(x_j \cos \beta + y_j \sin \beta)} J_n(kr_j) e^{in(\pi/2 - \beta)} + C_n^j \frac{H_n(kr_j)}{H_n'(ka_j)} + \sum_{\substack{l=1 \\ l \neq j}}^N \sum_{m=-\infty}^{\infty} C_m^l \frac{a_l J_n(kr_j)}{a_l H_m'(ka_l)} H_{m-n}(kR_{lj}) e^{i(m-n)\alpha_{lj}} \right] \times \frac{\cosh kz}{\cosh kd} e^{in\theta_j} \quad (10)$$

The right-hand side of Eq. (10) represents the incident wave upon the  $j$ th cylinder, the scattered wave produced by the  $j$ th cylinder, and the re-scattered wave generated by the adjacent cylinder  $l$ , respectively.  $C_n^j$  is the unknown complex potential coefficient.  $H_n$  is the Hankel function of the first kind of order  $n$ , and  $H_n'$  is the first derivatives of the Hankel function, respectively.

In addition to applying the body boundary conditions associated with the free surface conditions, the present boundary value problem must satisfy the matching conditions at the interface between the regions, which are given by

$$\begin{aligned}\phi_1^j &= \phi_2^j \quad \text{on} \quad r_j = a_j, \quad d-h \leq z \leq d \\ \frac{\partial \phi_1^j}{\partial r} &= \frac{\partial \phi_2^j}{\partial r} \quad \text{on} \quad r_j = a_j, \quad d-h \leq z \leq d\end{aligned}\quad (11)$$

Substituting Eqs. (8) and (10), and using the orthogonality of depth from  $z=d-h$  to  $d$ , the first matching condition between region 1 and 2 in Eq. (11) can be rewritten as

$$\begin{aligned}& \sum_{n=-\infty}^{\infty} A_n^j \left\{ J_n(k_0 a_j) - \frac{J'_n(k_0 b_j)}{Y'_n(k_0 b_j)} Y_n(k_0 a_j) \right\} \int_{d-h}^d \left\{ \frac{\cosh\{k_0(z-d+h)\}}{\cosh(k_0 h)} \right\}^2 dz \\ &= \sum_{n=-\infty}^{\infty} \left[ e^{ik(x \cos \beta + y \sin \beta)} J_n(ka_j) e^{in(\pi/2 - \beta)} \right. \\ & \quad \left. + C_n^j \frac{H_n(ka_j)}{H'_n(ka_j)} + \sum_{l=1}^N \sum_{m=-\infty}^{\infty} C_m^l \frac{a_l J_n(ka_j)}{a_l H'_m(ka_j)} H_{m-n}(kR_{lj}) e^{i(m-n)\alpha_{lj}} \right] \times \int_{d-h}^d \left\{ \frac{\cosh kz \cosh\{k_0(z-d+h)\}}{\cosh kd \cosh(k_0 h)} \right\} dz\end{aligned}\quad (12)$$

Applying the orthogonal property to the second matching conditions in Eq. (11), with respect to  $z$  over the region of validity, the following equation can be obtained

$$\int_0^d \frac{\partial \phi_2^j}{\partial r} \left\{ \frac{\cosh kz}{\cos kd} \right\} dz = \int_0^{d-h} \frac{\partial \phi_2^j}{\partial r} \frac{\cosh kz}{\cos kd} dz + \int_{d-h}^d \frac{\partial \phi_1^j}{\partial r} \frac{\cosh kz}{\cos kd} dz\quad (13)$$

By applying Eq. (12) to Eq. (13), the key equation for unknown coefficients  $C_n^j$  can be obtained as follows

$$\begin{aligned}C_n^j & \left[ k \int_0^d \left\{ \frac{\cosh kz}{\cosh kd} \right\}^2 dz - \frac{\left\{ J'_n(k_0 a_j) - \frac{J'_n(k_0 b_j)}{Y'_n(k_0 b_j)} Y_n(k_0 a_j) \right\} k_0}{\left\{ J_n(k_0 a_j) - \frac{J'_n(k_0 b_j)}{Y'_n(k_0 b_j)} Y_n(k_0 a_j) \right\}} \times \frac{H_n(ka_j)}{H'_n(ka_j)} H_n(ka_j) \right. \\ & \quad \left. \times \frac{\int_{d-h}^d \left\{ \frac{\cosh k_0(z-d+h) \cosh kz}{\cosh k_0 h \cosh kd} \right\} dz \times \int_{d-h}^d \left\{ \frac{\cosh k_0(z-d+h) \cosh kz}{\cosh k_0 h \cosh kd} \right\} dz}{\int_{d-h}^d \left\{ \frac{\cosh k_0(z-d+h)}{\cosh k_0 h} \right\}^2 dz} \right] \\ & + \sum_{l=1}^N \sum_{m=-\infty}^{\infty} C_m^l \frac{a_l H_{m-n}(kR_{lj})}{a_l H'_m(ka_l)} e^{i(m-n)\alpha_{lj}} \times J'_n(ka_j) k \int_0^d \left\{ \frac{\cosh kz}{\cosh kd} \right\}^2 dz\end{aligned}$$

$$\begin{aligned}
& - \sum_{l=j}^N \sum_{m=-\infty}^{\infty} C_m^l \frac{a_l H_{m-n}(kR_{lj})}{a_l H_m'(ka_l)} e^{i(m-n)\alpha_{lj}} \times J_n(ka_j) \\
& \times \left[ \frac{\left\{ J_n'(k_0 a_j) - \frac{J_n'(k_0 b_j)}{Y_n'(k_0 b_j)} Y_n'(k_0 a_j) \right\} k_0 \int_{d-h}^d \left\{ \frac{\cosh k_0(z-d+h)}{\cosh k_0 h} \frac{\cosh kz}{\cosh kd} \right\} dz \times \int_{d-h}^d \left\{ \frac{\cosh k_0(z-d+h)}{\cosh k_0 h} \frac{\cosh kz}{\cosh kd} \right\} dz}{\left\{ J_n(k_0 a_j) - \frac{J_n'(k_0 b_j)}{Y_n'(k_0 b_j)} Y_n(k_0 a_j) \right\} \int_{d-h}^d \left\{ \frac{\cosh k_0(z-d+h)}{\cosh k_0 h} \right\}^2 dz} \right] \\
& = -e^{ik(x_j \cos \beta + y_j \sin \beta)} e^{in(\pi/2 - \beta)} \left[ \frac{J_n'(ka_j) k \int_0^d \left\{ \frac{\cosh kz}{\cosh kd} \right\}^2 dz - \left\{ J_n'(k_0 a_j) - \frac{J_n'(k_0 b_j)}{Y_n'(k_0 b_j)} Y_n'(k_0 a_j) \right\} k_0}{\left\{ J_n(k_0 a_j) - \frac{J_n'(k_0 b_j)}{Y_n'(k_0 b_j)} Y_n(k_0 a_j) \right\}} J_n(ka_j)} \right. \\
& \left. \times \frac{\int_{d-h}^d \left\{ \frac{\cosh k_0(z-d+h)}{\cosh k_0 h} \frac{\cosh kz}{\cosh kd} \right\} dz \times \int_{d-h}^d \left\{ \frac{\cosh k_0(z-d+h)}{\cosh k_0 h} \frac{\cosh kz}{\cosh kd} \right\} dz}{\int_{d-h}^d \left\{ \frac{\cosh k_0(z-d+h)}{\cosh k_0 h} \right\}^2 dz} \right] \quad (14)
\end{aligned}$$

In order to calculate the potential coefficients  $C_n^j$  from the infinite system, Eq. (14) is truncated to  $(2M+1)N$  equations with  $(2M+1)N$  unknown values for  $j=1, 2, \dots, N$  and  $n=-M, \dots, M$ . That is,

$$\begin{aligned}
& C_n^j \left\{ kS_1 - \frac{Q_1 k_0 S_2}{Q_2 S_3} \frac{H_n(ka_j)}{H_n'(ka_j)} H_n(ka_j) \right\} \\
& + \sum_{l=j}^N \sum_{m=-M}^M C_m^l \frac{a_l H_{m-n}(kR_{lj})}{a_l H_m'(ka_l)} e^{i(m-n)\alpha_{lj}} \left\{ J_n'(ka_j) kS_1 - \frac{Q_1 k_0 S_2}{Q_2 S_3} J_n(ka_j) \right\} \\
& = -e^{ik(x_j \cos \beta + y_j \sin \beta)} e^{in(\pi/2 - \beta)} \left\{ J_n'(ka_j) kS_1 - \frac{Q_1 k_0 S_2}{Q_2 S_3} J_n(ka_j) \right\} \quad (15)
\end{aligned}$$

where

$$S_1 = \int_0^d \left\{ \frac{\cosh kz}{\cosh kd} \right\}^2 dz$$

$$S_2 = \int_{d-h}^d \left\{ \frac{\cosh k_0(z-d+h)}{\cosh k_0 h} \frac{\cosh kz}{\cosh kd} \right\} dz \times \int_{d-h}^d \left\{ \frac{\cosh k_0(z-d+h)}{\cosh k_0 h} \frac{\cosh kz}{\cosh kd} \right\} dz$$

$$S_3 = \int_{d-h}^d \left\{ \frac{\cosh k_0(z-d+h)}{\cosh k_0 h} \right\}^2 dz$$

$$Q_1 = \left\{ J_n'(k_0 a_j) - \frac{J_n'(k_0 b_j)}{Y_n'(k_0 b_j)} Y_n'(k_0 a_j) \right\}$$

$$Q_2 = \left\{ J_n(k_0 a_j) - \frac{J'_n(k_0 b_j)}{Y'_n(k_0 b_j)} Y_n(k_0 a_j) \right\}$$

By using a stand matrix technique, the equations on  $C_n^j$  can be solved and the unknown coefficients  $A_n^j$  may then be obtain from Eq. (12) by applying  $C_n^j$ . In this manner the velocity potential in each fluid region ( $\phi_1^j, \phi_2^j$ ) can be determined.

After solving the velocity potentials, the wave excitation forces on each cylinder are obtained using the integration of pressure on the wetted surface of cylinder. Wave forces in x-direction ( $F_x$ ) and in y-direction ( $F_y$ ) are calculated as follows

$$\begin{aligned} F_x^j &= -i\rho\omega \int_{d-h}^d \int_0^{2\pi} \frac{-igH}{2\omega} \{\phi_1^j\} b_j \cos \theta d\theta dz \quad \text{on} \quad d-h \leq z \leq d \\ F_y^j &= -i\rho\omega \int_{d-h}^d \int_0^{2\pi} \frac{-igH}{2\omega} \{\phi_1^j\} b_j \sin \theta d\theta dz \quad \text{on} \quad d-h \leq z \leq d \end{aligned} \quad (16)$$

$$\begin{aligned} F_x^j &= -i\rho\omega \int_0^{d-h} \int_0^{2\pi} \frac{-igH}{2\omega} \{\phi_2^j\} a_j \cos \theta d\theta dz \quad \text{on} \quad 0 \leq z \leq d-h \\ F_y^j &= -i\rho\omega \int_0^{d-h} \int_0^{2\pi} \frac{-igH}{2\omega} \{\phi_2^j\} a_j \sin \theta d\theta dz \quad \text{on} \quad 0 \leq z \leq d-h \end{aligned} \quad (17)$$

where Eq. (16) is for upper part and Eq. (17) is for lower part of the hybrid substructure with multi-cylinder.

### 3. Numerical results and discussion

In order to verify the wave forces on an array of four cylinders, the present numerical results are compared with the numerical results of Williams and Li (2000) for the various incident wave angles ( $\beta$ ). The calculation conditions are  $a=10.0$  m and  $d=50.0$  m. The cylinders are numbered clockwise from 1 to 4 and situated at  $(-20, 20)$  m,  $(20, 20)$  m,  $(20, -20)$  m, and  $(-20, -20)$  m, respectively. The wave forces are normalized by  $\rho g(H/2)a^2$  and the axis of abscissa denotes the wave number. Although the wave number at the first peak value of wave force is very similar for all cases, the wave number at the second peak becomes different according to the incident wave angles. The calculated wave forces obtained from the present method are in good agreement with the results from Williams and Li (2000) as shown in Fig. 2.

Fig. 3 show the comparison of wave forces on hybrid substructure with five cylinders for various depths ( $h/d$ ) of region 1. The calculation conditions are  $a_1=3.0$  m,  $b_1=1.0$  m,  $a_j=1.0$  m,  $b_j=0.5$  m ( $j=2,3,4,5$ ) and  $d=20.0$  m. The largest cylinder 1 is located at  $(0, 0)$  m, and the other cylinders are numbered clockwise from 2 to 5 and situated at  $(-4, 0)$  m,  $(0, -4)$  m,  $(4, 0)$  m, and  $(0, -4)$  m, respectively. In the comparison the ratio of  $h/d=0.0$  indicates the case without small cylinders of region 1, while  $h/d=1.0$  represents the case with only small cylinders. The calculated total wave forces are normalized by  $\rho g(H/2)a_1^2$ . In the comparison, the peak wave force with depth 0.25 and 0.5 decreases about 33% and 50%, respectively, compared to the peak value of depth 1.0. Although in the long wave region ( $ka \leq 0.8$ ) the pattern of wave forces is strongly influenced by the

depth of region 1, the pattern of both depth 0.5 and 0.0 becomes very similar, and the difference between depth 0.5 and 1.0 is very small in the short wave region ( $ka \geq 0.8$ ). The wave forces on the hybrid substructure with the depth 0.25 become remarkably smaller than those on the mono pile with radius 3.0 m as the wave number becomes larger than 0.6. It means that the hybrid substructure with depth 0.25 of region 1 is significantly efficient to reduce the wave forces acting on hybrid substructures in the short wave region.

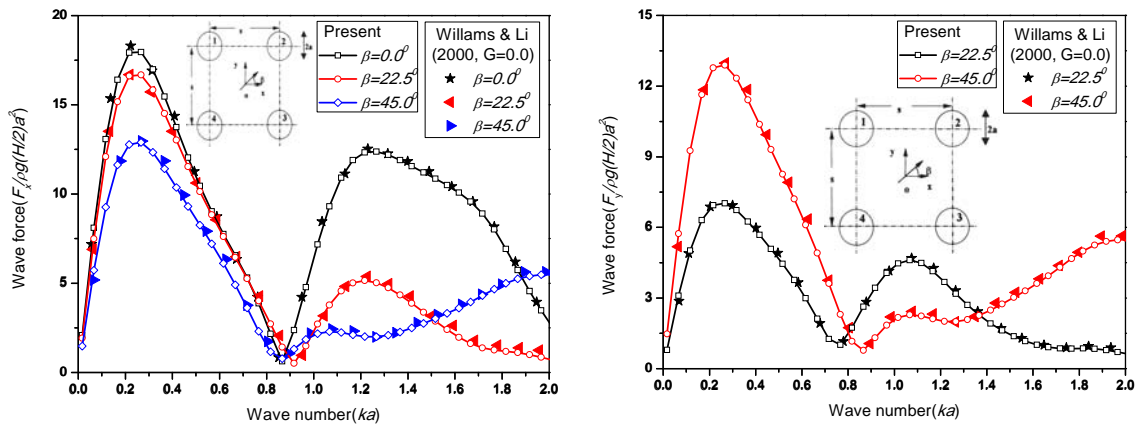


Fig. 2 Comparison of wave forces on the array of four cylinders with Williams and Li (2000) for  $d/a=5$  and  $s/a=4$

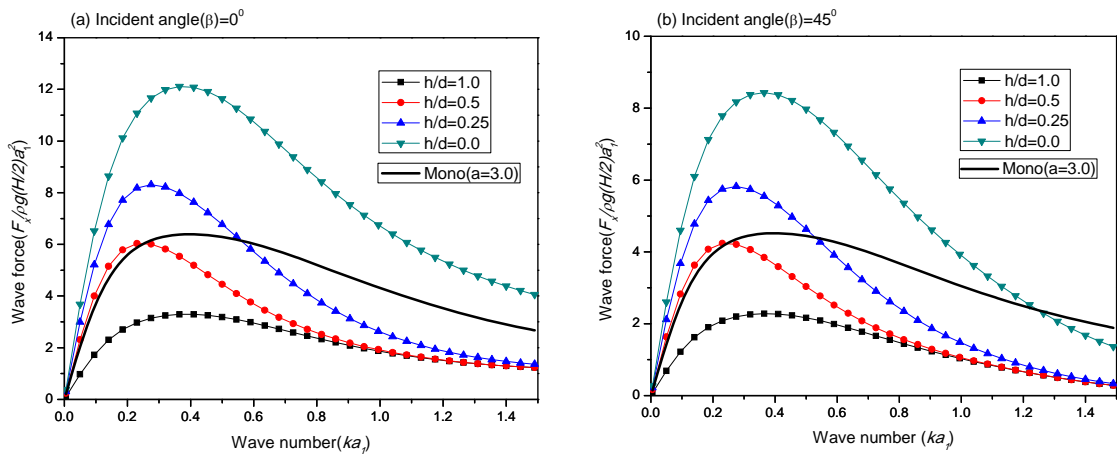


Fig. 3 Comparison of total wave forces on the hybrid substructure of five cylinders with  $a_1=3.0$  m,  $b_1=1.0$  m,  $a_j=1.0$  m,  $b_j=0.5$  m ( $j=2,3,4,5$ ) and  $d=20.0$  m for various depths ( $h/d$ ): (a) x-direction for  $\beta=0.0^\circ$  and (b) x-direction for  $\beta=45.0^\circ$

The wave forces on each cylinder of the hybrid substructure with five cylinders are presented in Fig. 4. In case of incident wave angle  $0.0^\circ$ , the wave forces on cylinder 1 are largest and the wave forces on cylinder 3 and 5 have same values. The pattern of cylinder 3 and 5 in x-direction shows the same pattern of cylinder 4 and 2 in y-direction in case of incident wave angle  $45^\circ$ .

Fig. 5 shows the comparison of total wave forces on the hybrid substructure with five cylinders for various radiuses ( $b_1$ ) of cylinder 1. Since the wave force is closely related to the wetted surface of structure, the wave forces gradually decrease as the radius of cylinder 1 decreases. The hybrid substructure with the radius less than  $2.0\text{ m}$  is significantly efficient to reduce the wave forces in short wave region ( $ka \geq 0.7$ ) compared to the mono pile with radius  $3.0\text{ m}$ .

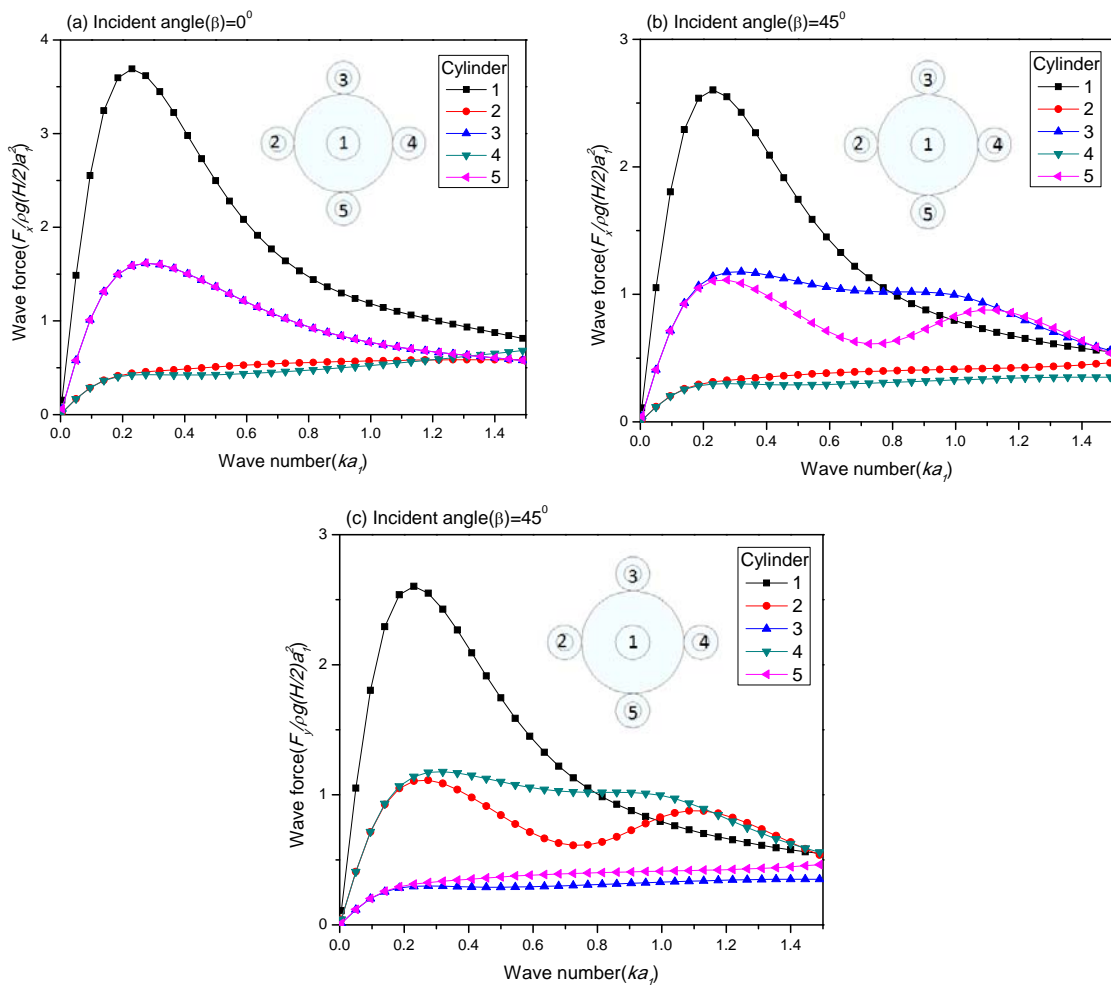


Fig. 4 Comparison of wave forces on each cylinder with  $a_1=3.0\text{ m}$ ,  $b_1=1.0\text{ m}$ ,  $a_j=1.0\text{ m}$ ,  $b_j=0.5\text{ m}$  ( $j=2,3,4,5$ ) and  $d=20.0\text{ m}$  for various incident wave angles ( $\beta$ ): (a) x-direction for  $\beta=0.0^\circ$ , (b) x-direction for  $\beta=45.0^\circ$  and (c) y-direction for  $\beta=45.0^\circ$

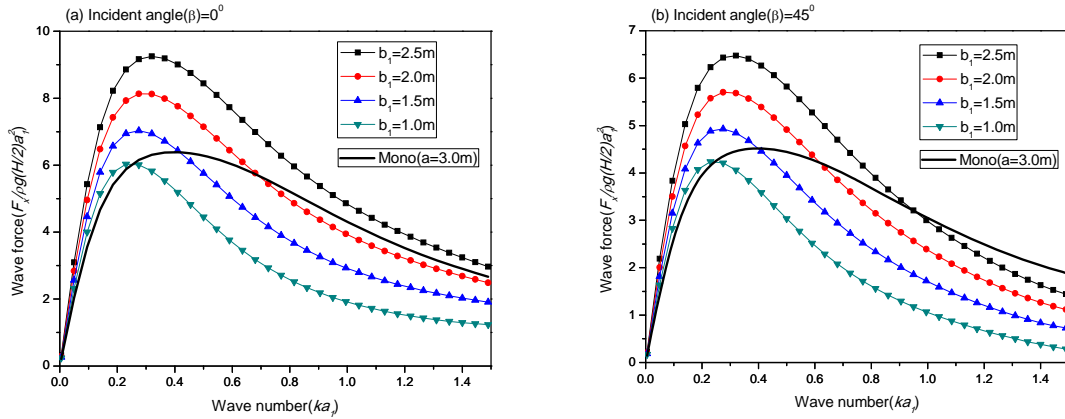


Fig. 5 Comparison of total wave forces on the hybrid substructure of five cylinders with  $a_1=3.0$  m,  $a_j=1.0$  m,  $b_j=0.5$  m ( $j=2,3,\dots,5$ ) and  $d=20.0$  m for various radiuses of cylinder 1 ( $b_1$ ): (a) x-direction for  $\beta=0.0^\circ$  and (b) x-direction for  $\beta=45.0^\circ$

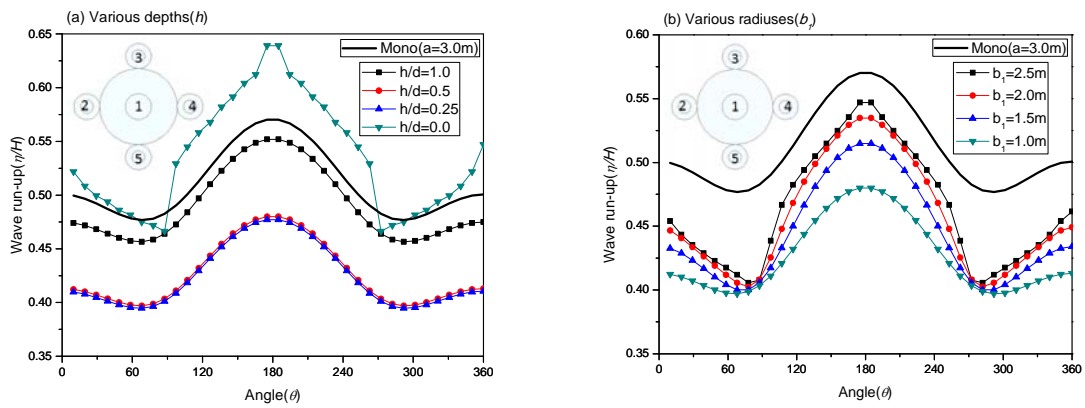


Fig. 6 Comparison of wave run-ups on cylinder 1 for five cylinders with  $\beta=0.0^\circ$  and  $ka=0.3$ : (a) Various depths ( $h/d$ ) with  $b_1=1.0$  m and (b) Various radiuses ( $b_j$ ) with  $h/d=0.5$

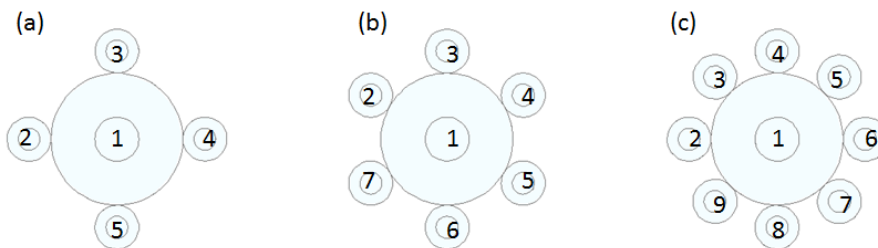


Fig. 7 Hybrid substructure: (a) Five cylinders, (b) Seven cylinders, (c) Nine cylinders

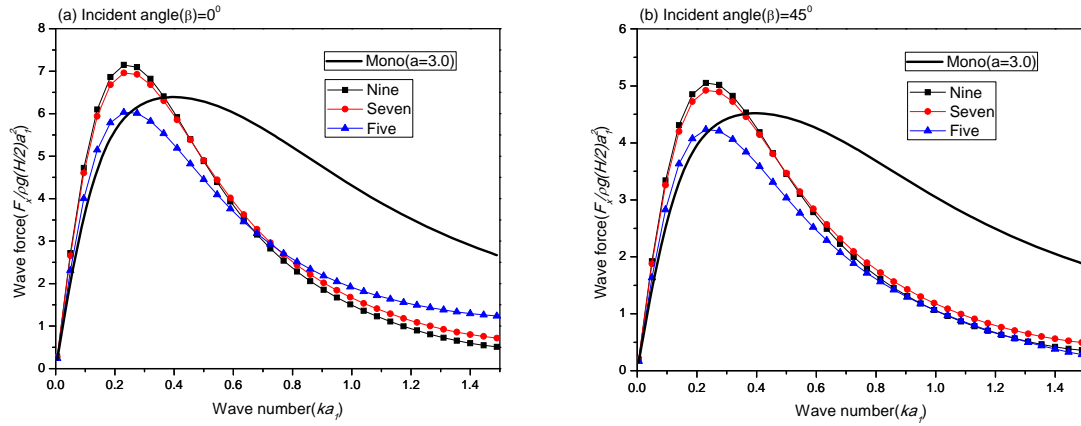


Fig. 8 Comparison of total wave forces on the hybrid substructure of various cylinder numbers with  $a_1=3.0$  m,  $b_1=1.0$  m,  $a_j=1.0$  m,  $b_j=0.5$  m ( $j=2,3,\dots,7$ ) and  $d=20.0$  m for various incident wave angles ( $\beta$ ): (a) x-direction for  $\beta=0.0^\circ$  and (b) x-direction for  $\beta=45.0^\circ$

Fig. 6 shows the comparison of wave run-up on cylinder 1 for five cylinders with the incident wave angle ( $\beta$ )  $0.0^\circ$ . Since the wave force has the peak value when the wave number is 0.3, the comparison of wave run-ups is made at the wave number 0.3. The calculation conditions are  $a_1=3.0$  m,  $a_j=1.0$  m,  $b_j=0.5$  m ( $j=2,3,4,5$ ) and  $d=20.0$  m. The wave run-up is normalized by incident wave height ( $H$ ) and the abscissa denotes the angle ( $\theta$ ) measured counter-clockwise from the positive x-axis. The wave run-up on cylinder 1 is largest when the depth of region 1 is 0.0. However, in case of depth 1.0 with only small cylinders the wave run-up is smaller than that of depth 0.0 and the mono pile with radius 3.0 m. Although the difference of wave run-up between the depth 0.25 and 0.5 is small, the wave run-up on hybrid substructure is smallest for all cases. It means that the suggested hybrid substructure remarkably reduce the wave run-up on cylinder 1. Although the wave run-up due to the radius of cylinder 1 is gradually increased as the radius of cylinder 1 increases, it is smaller than in case of the mono pile with radius 3.0 m for all cases. It means that the suggested hybrid substructure plays very important role to reduce the wave forces and wave run-up compared to the mono pile at the penalty of increased cost.

The Comparison of total wave forces on the hybrid substructure of various cylinder numbers is presented in Fig. 8 to examine the water wave interaction among cylinders. The relative contributions of viscous drag forces for various shapes, particularly in the long wave regime, are beyond the scope of the present study. The calculation conditions are  $a_1=3.0$  m,  $b_1=1.0$  m,  $h/d=0.5$ ,  $a_j=1.0$  m,  $b_j=0.5$  m ( $j=2,3,\dots,9$ ) and  $d=20.0$  m. The largest cylinder 1 is located at center, and the other cylinders are numbered clockwise from 2 to 9 as shown in Fig. 7. In the long wave region ( $ka \leq 0.7$ ) the peak wave force of nine cylinders is largest and the difference of peak wave force between seven and nine cylinders is small. The wave forces of nine cylinders gradually decrease and especially have a lower value than those of five cylinders in the short wave region ( $ka \geq 0.7$ ). The difference between five and nine cylinders becomes larger as the wave number is greater than 0.7. It means that wave forces are strongly influenced by the wave length and the water wave interaction is strongly depended on the relation between the wave length and the number of cylinders. Moreover, the wave forces acting on the suggested hybrid substructure is smaller than

those on the mono pile with radius 3.0 m when the wave number is larger than 0.4. It means that the hybrid substructure is significantly efficient to reduce the wave forces compared to the mono pile in the short wave region.

The wave forces on each cylinder of hybrid substructure with seven and nine cylinders are shown in Figs. 9 and 10. The wave force on cylinder 1 is largest for all cases.

Fig. 11 shows the comparison of wave run-up on each cylinder for various hybrid substructures. The wave run-up on the cylinder 2 for both cases of five and nine cylinders has the similar pattern since the incident wave propagates toward the cylinder 2. The peak value of cylinder 1 is lowest in all cases. It is found that due to the reduction of wave-body interaction the wave run-up of cylinder 1 has a similar value regardless of the number of cylinders and the hybrid substructures, when the depth ratio of region 1 becomes a larger than 50.0% of whole water depth ( $h/d=0.5$ ), is remarkably effective to reduce the wave run up.

Fig. 12 shows the non-dimensional elevation contours on hybrid substructure of various cylinder members at the wave number 0.3.

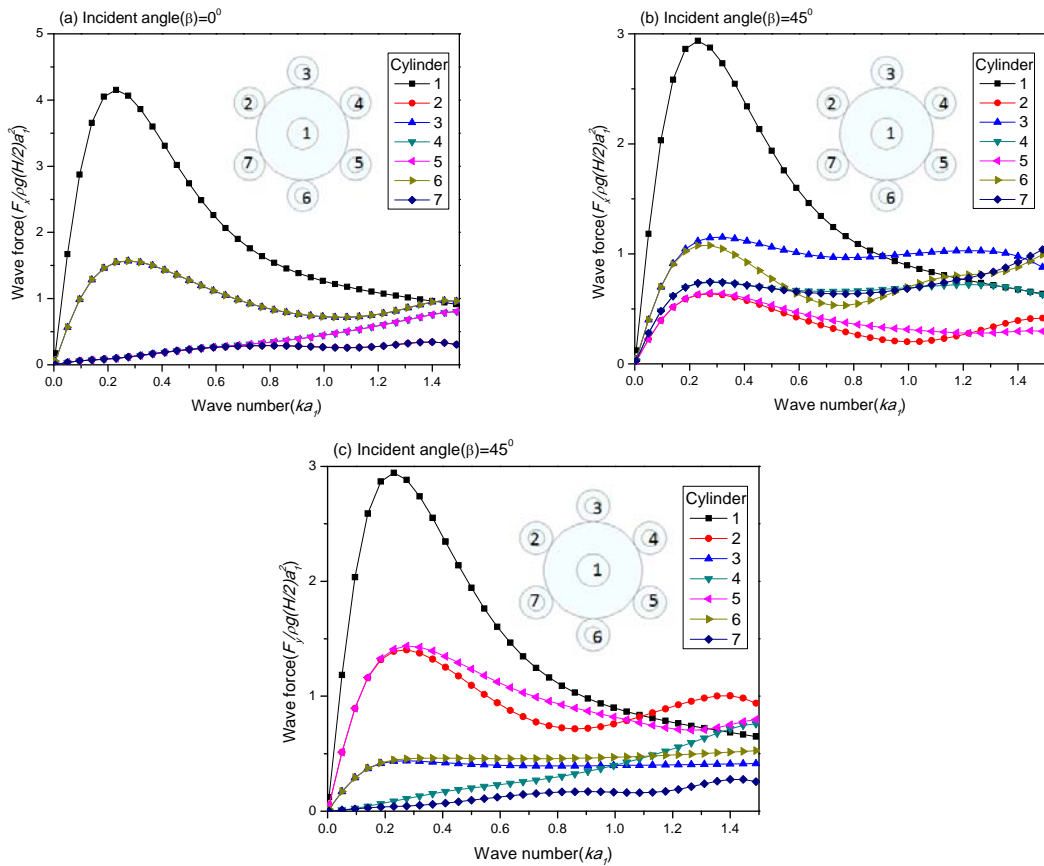


Fig. 9 Comparison of wave forces on each cylinder with  $a_1=3.0$  m,  $b_1=1.0$  m,  $a_j=1.0$  m,  $b_j=0.5$  m ( $j=2,3,\dots,7$ ) and  $d=20.0$  m for various incident wave angles ( $\beta$ ): (a) x-direction for  $\beta=0.0^\circ$ , (b) x-direction for  $\beta=45.0^\circ$  and (c) y-direction for  $\beta=45.0^\circ$

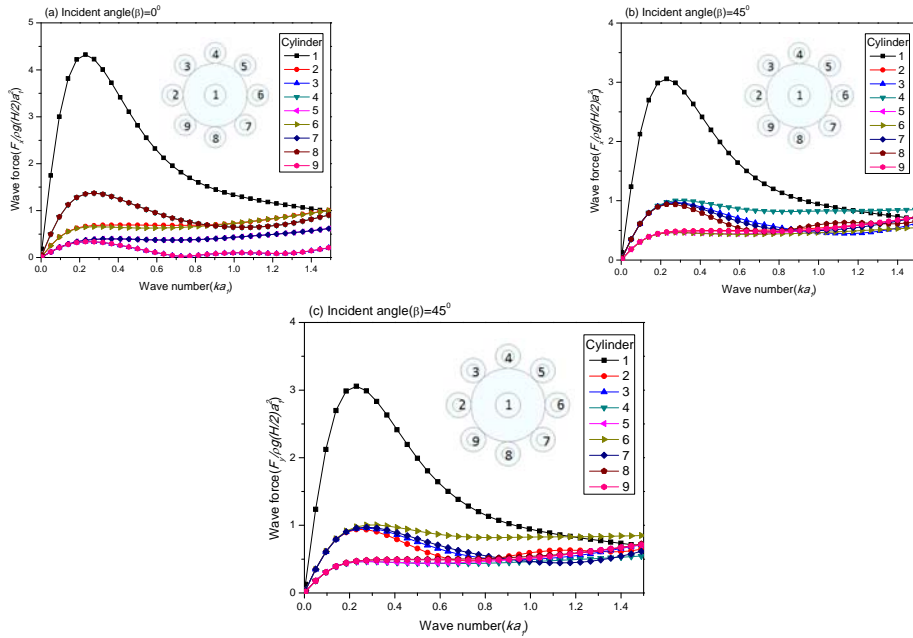


Fig. 10 Comparison of wave forces on each cylinder with  $a_I=3.0$  m,  $b_I=1.0$  m,  $a_j=1.0$  m,  $b_j=0.5$  m ( $j=2,3,\dots,9$ ) and  $d=20.0$  m for various incident wave angles ( $\beta$ ): (a) x-direction for  $\beta=0.0^\circ$ , (b) x-direction for  $\beta=45.0^\circ$  and (c) y-direction for  $\beta=45.0^\circ$

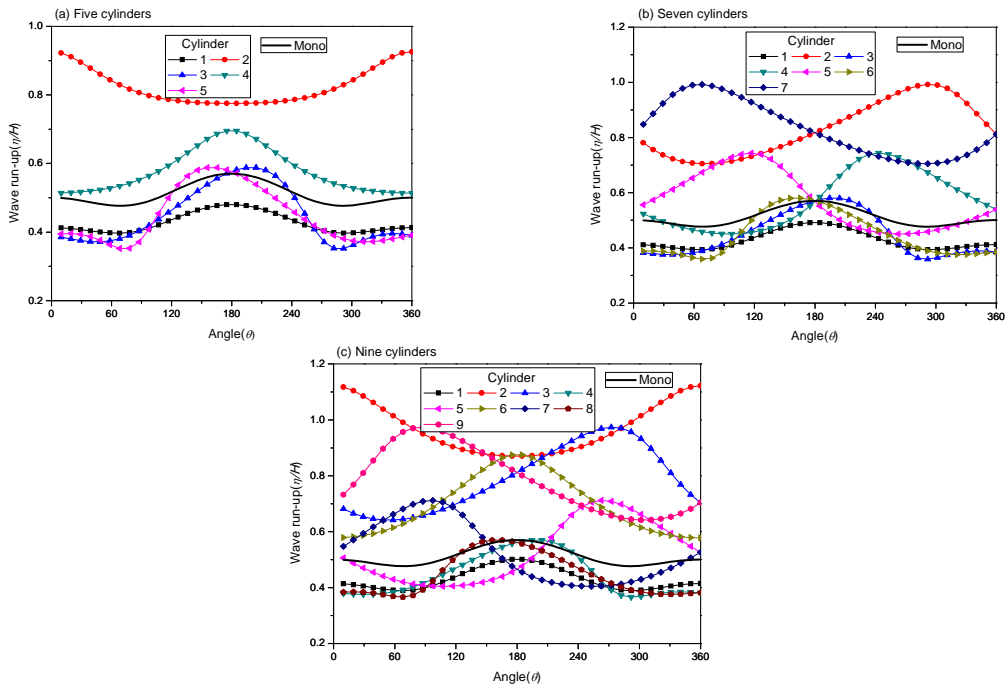


Fig. 11 Comparison of wave run-ups on hybrid substructure of various cylinder numbers with  $\beta=0.0^\circ$ ,  $h/d=0.5$  and  $ka=0.3$ : (a) Five cylinders, (b) Seven cylinders and (c) Nine cylinders

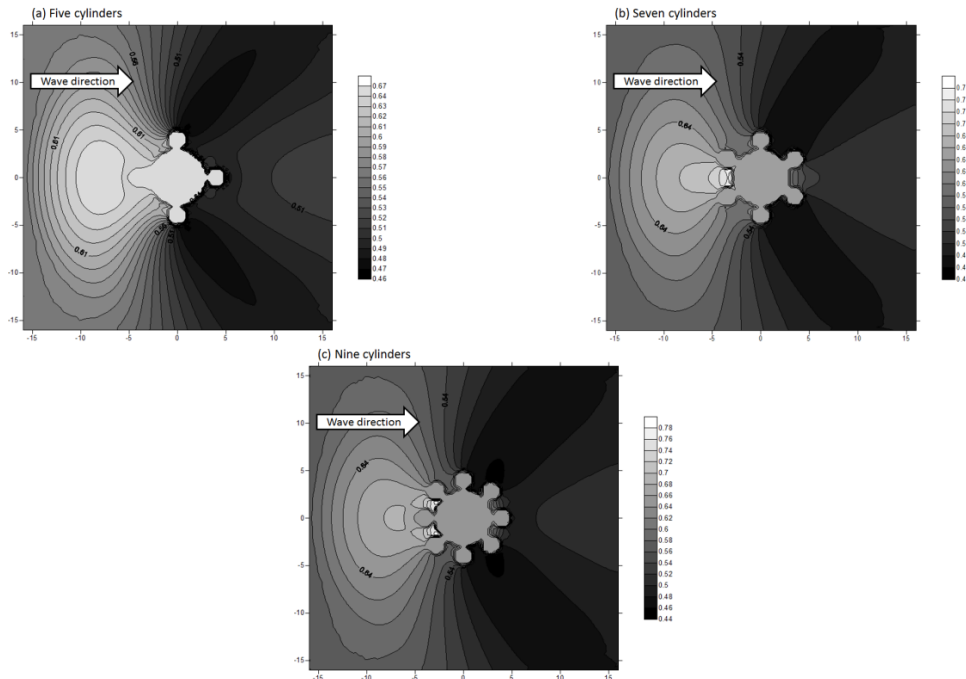


Fig. 12 Free surface elevation contours around hybrid substructure for various cylinder numbers with  $\beta=0.0^\circ$ ,  $h/d=0.5$  and  $ka=0.3$ : (a) Five cylinders, (b) Seven cylinders and (c) Nine cylinders

## 5. Conclusions

The hybrid substructure with multi-cylinder for offshore wind turbines is newly suggested to reduce the wave forces on substructures. Under the assumption of potential flow and linear wave theory, a 3D numerical method for the hybrid substructure was developed using the Eigen-function expansion method. In the short wave region, the wave force on hybrid substructures is found to be greatly reduced compared to the case without small cylinder of region 1. Consequently, installing small cylinders of region 1 on the gravity substructure may be an effective means of decreasing the wave forces. It is also found that the suggested hybrid substructure with depth ratio 0.25 of region 1 effectively reduces the wave force compared to the mono pile in the short wave region. Moreover the water wave interactions among cylinders rapidly diminish for the hybrid substructure. It means that the hybrid substructure significantly reduces the wave run-up on substructure. Consequently, the suggested hybrid substructure for offshore wind turbines with multi-cylinder can be an effective substructure for reducing hydrodynamic effects in the short wave region.

## Acknowledgments

This study was supported by the Korea Institute of Energy Technology Evaluation and Planning through the research project “Development of hybrid substructure systems for offshore wind

power (2012T100201671)".

## References

- Abramowitz, M. and Stegun, I.A. (1972), *Handbook of mathematical functions*, Dover Publications, New York.
- Cho, I.H. and Kim, M.H. (2010), "Wave deformation and blocking performance by N porous bottom-mounted vertical circular cylinders", *Int. J. Offshore Polar.*, **20**(4), 284-291.
- Cho, I.H., Kim, M.H. and Kweon, H.M. (2012), "Wave energy converter by using relative heave motion between buoy and inner dynamic system", *Ocean Syst. Eng.*, **2**(4), 297-314.
- Kagemoto, H. and Yue, D.K.P. (1986), "Interactions among multiple three-dimensional bodies in water waves; an exact algebraic method", *J. Fluid Mech.*, **166**, 189-209.
- Kim, M.H. (1993), "Interaction of waves with N vertical circular cylinders", *J. Waterw. Port C - ASCE.*, **119**(6), 671-689.
- Linton, C.M. and Evans, D.V. (1990), "The interaction of waves with arrays of vertical circular cylinder", *J. Fluid Mech.*, **215**, 549-569.
- McIver, P. (1984), "Wave forces on arrays of floating bodies", *J. Eng. Math.*, **18**(4), 273-285.
- McIver, P. and Evans, D.V. (1984), "Approximation of wave forces on cylinder arrays", *Appl. Ocean Res.*, **6**(2), 101-107.
- Park, M.S., Koo, W.C. and Choi, Y.R. (2010), "Hydrodynamic interaction with an array of porous circular cylinders", *Int. J. Naval Architecture and Ocean Eng.*, **2**(3), 146-154.
- South Korea offshore wind project plan (2011), <<http://www.evwind.es/2011/11/13/south-korea-to-build-worlds-largest-offshore-wind-farm/>>.
- Spring, B.H. and Monkmeyer, P.L. (1974), "Interaction of plane waves with vertical cylinders", *Proceedings of the 14th International Conference on Coastal Engineering*.
- Williams, A.N. and Abul-Azm, A.G. (1989), "Hydrodynamic interactions in floating cylinder arrays; Part II-Wave radiation", *Ocean Eng.*, **16**(3), 217-264.
- Williams, A.N. and Demirbilek, Z. (1988), "Hydrodynamic interactions in floating cylinder arrays; Part I-Wave scattering", *Ocean Eng.*, **15**(6), 549-583.
- Williams, A.N. and Li, W. (1998), "Wave interaction with a semi-porous cylindrical breakwater mounted on a storage tank", *Ocean Eng.*, **25**(2-3), 195-219.
- Williams, A.N. and Li, W. (2000), "Wave interaction with an array of bottom-mounted surface-piercing porous cylinders", *Ocean Eng.*, **27**(8), 841-866.
- Williams, A.N., and Rangappa, T. (1994), "Approximate hydro-dynamic analysis of multi-column ocean structures", *Ocean Eng.*, **21**(6), 519-573.
- Zhao, F., Bao, W., Kinoshita, T. and Itakura, H. (2011), "Theoretical and experimental study on a porous cylinder floating in waves", *J. Offshore Mech. Arct.*, **133**(1), 301-311.

It is noted that this paper is revised edition based on The 2013 World Congress on Advances in Structural Engineering and Mechanics, September 8-12, 2013, Korea.